Macromolecules

Article

pubs.acs.org/Macromolecules

Two-Dimensional Subnanometer Confinement of Ethylene Glycol and Poly(ethylene oxide) by Neutron Spectroscopy: Molecular Size Effects

Fabienne Barroso-Bujans,*[,†] Felix Fernandez-Alonso,[‡,∥] Silvina Cerveny,[†] Silvia Arrese-Igor,[†] Angel Alegría,[†,§] and Juan Colmenero[†,§,⊥]

[†]Centro de Física de Materiales-Material Physics Center (CSIC-UPV/EHU), Paseo Manuel Lardizábal 5, 20018 San Sebastián, Spain

[‡]ISIS Facility, Rutherford Appleton Laboratory, Chilton, Didcot, Oxfordshire OX11 0QX, U.K.

[§]Departamento de Física de Materiales, Universidad del País Vasco (UPV/EHU), Apartado 1072, 20080 San Sebastián, Spain

[⊥]Donostia International Physics Center, Paseo Manuel Lardizábal 4, 20018 San Sebastián, Spain

[∥]Department of Physics and Astronomy, University College London, Gower Street, London, WC1E 6BT, U.K.

Supporting Information

ABSTRACT: We explore the effects of chain size on the structure and dynamics of ethylene glycol (EG) and poly(ethylene oxide) (PEO) intercalated in graphite oxide (GO). To this end, EG as well as a PEO series of increasing chain length have been studied by means of high-resolution inelastic neutron spectroscopy. The neutron experiments are complemented by X-ray diffraction, differential scanning calorimetry, Fourier-transform infrared spectroscopy, and Raman scattering. We find that EG is accommodated in a layer of thickness ∼3 Å within the GO substrate and adopts a preferential, yet largely disordered, gauche conformation. Longer PEO chains give rise to a layer thickness in the range ∼3.0−3.4 Å characterized by planar zigzag (trans−trans−trans) conformations. Moreover, we observe a strong reduction of vibrational motions for the confined EG and polymer phases, as clearly evidenced by the disappearance, shift, and/or broadening of mode-specific inelastic neutron scattering spectral features, as well as by the complete suppression of crystallization. All of these effects are surprisingly insensitive to the length of the PEO chains.

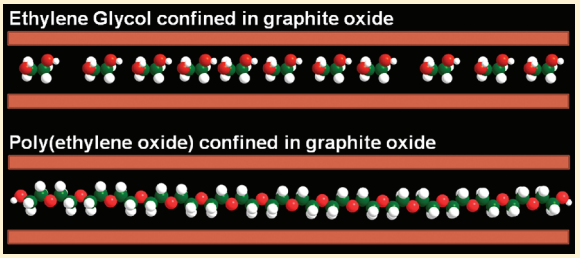

INTRODUCTION

Following the seminal works of McKenna and co-workers,[1,2] many studies on the dynamics of glass-forming liquids subjected to nanoscale confinement have noted a size-dependent reduction in glass-transition temperatures (T_g) which could not be readily explained by conventional theories. Subsequent work has shown that T_g can also increase, remain the same, or even disappear upon confinement.[3] In spite of a plethora of experimental and theoretical studies over the past 2 decades, the influence of spatial confinement on polymer dynamics is still poorly understood and a matter of heated debate. A major obstacle to further progress lies in the difficulties associated with the synthesis of materials with well-defined confining geometries. In this context, graphite oxide (GO) offers a novel means of studying the structure and dynamics of intercalated molecules and macromolecules confined within well-defined two-dimensional (2D) layers of subnanometer dimensions. Pristine GO provides a layered structure characterized by an interlayer spacing of 5.7 Å and it is highly hydrophilic. It can accommodate water[4] as well as other solvent molecules (including methanol, 1-propanol, 1-pentanol, 1-hexanol, benzene, toluene, *p*-xylene, chlorobenzene, CH_2Cl_2, $CHCl_3$)[5,6] between its layers with a surprisingly high degree of interplanar long-range order along the crystallographic *c*-axis.

In a recent study on the intercalation of high-molecular-weight (∼10^5 g/mol) poly(ethylene oxide) (PEO) in GO, we have shown intriguing effects on the structure and dynamics of the confined PEO phase.[7] In essence, we found no evidence of crystallization or glass-transition associated with the confined polymer. For the first time, high-resolution inelastic neutron scattering (INS) provided a direct link between these stark changes in macroscopic behavior and the underlying conformation of the 2D organic phase. Certainly, the conformational changes experienced by PEO as a function of surrounding conditions (i.e., salt addition, pore size, temperature, etc.) have been reported in previous studies using solid-state nuclear magnetic resonance (NMR) as well as Fourier-transform infrared (FTIR) spectroscopy and Raman scattering.[8−17] However, these spectroscopic techniques typically suffer from a strong interference from the substrate. Owing to the strong neutron−proton incoherent cross section, INS

Received: December 7, 2011
Revised: March 12, 2012

dx.doi.org/10.1021/ma202655f | Macromolecules XXXX, XXX, XXX−XXX

circumvents these difficulties in the characterization of the confined hydrogeneous phase, with minimal interference from the graphitic substrate.[18] Additionally, INS provides access to a broad range of energy transfers, from those associated with stochastic and intermolecular modes in the hard-to-reach terahertz frequency range (1 THz = 33 cm^{-1}), to those characteristic of strong chemical bonds all the way up to 4000 cm^{-1}.

The conformation adopted by PEO upon 2D confinement depends quite critically on the chemical nature of the substrate. For example, PEO intercalated in smectic clays has been hypothesized to form helices capable of accommodating interlayer cations in their cores.[12] However, subsequent computer simulations strongly suggested that such a helical conformation is highly distorted and that the cations reside next to the silicate surface rather than being coordinated to the confined polymer.[19] Likewise, preferential planar conformations have been suggested for PEO and its smaller molecular-weight analogue poly(ethylene glycol) (PEG) confined in kaolinite,[11] V_3O_8,[20] and V_2O_5 interlayers.[21] A bilayer PEO arrangement of thickness 8.3 Å has also been suggested for confinement in the inorganic layered material MoS_2,[22] whereas a more detailed study by means of solid-state NMR has estimated that most of the PEO chains are accommodated with a large fraction of OC−CO bonds (∼90%) in a gauche conformation.[8] On the basis of these results, helical conformations are still expected to be the preferential structure of the confined polymer, as it is the case in the bulk material. Furthermore, the strong electrostatic interactions with mobile cations such as K^+, Li^+, and Na^+ ubiquitous in clays and other layered minerals are likely to dictate both the structural and dynamical behavior of the confined polymer phase.[8−10,19,23,24] This is not the case of GO, as it is ion-free and its simple chemical composition (only involving C, O, and H) translates into a far better-defined composite material for fundamental studies of direct relevance to the development of novel technologies.

As mentioned above, high-molecular-weight PEO chains (∼10^5 g/mol) intercalate into GO layers giving rise to a well-defined polymer layer of thickness ∼3.4 Å and bulk-like areal densities.[7] In this extremely restricted planar geometry, INS has established that the confined macromolecule adopts a preferential planar zigzag conformation, signifying a strong departure from the intramolecular structure of the bulk. Motivated by these new results, the present work explores how macromolecular structure evolves in PEO/GO intercalates as a function of intercalant size. To this end, we have synthesized a series of PEO/GO samples of increasing PEO chain length [HO−$(CH_2CH_2O)_n$−H], where n = 3, 5, 13, 104, 795, and 2135 (hereafter we will use the term "nPEO" to identify the "n" chain length of each PEO used). Note also that we have used the term PEO indistinctly from PEG because it is difficult to establish at which point PEG becomes PEO or vice versa. To complete this chemical series, ethylene glycol (EG, n = 1) was also studied. INS provided access to the entire vibrational density of states (VDOS) of the confined organic phase as a function of chain length over a wide energy-transfer range. The INS data were collected on the TOSCA spectrometer[25] located at the ISIS Facility, Rutherford Appleton Laboratory, U.K. These data were complemented by further measurements using X-ray diffraction (XRD), thermogravimetric analysis (TGA), differential scanning calorimetry (DSC), Fourier-transform infrared spectroscopy (FTIR), and Raman scattering. The experimental results reveal a strong reduction of vibrational motions of the chain for the confined EG and polymer phases, as clearly evidenced by the disappearance, shift, and/or broadening of mode-specific INS bands, as well as by the complete suppression of crystallization. The INS data also account for profound conformational changes taking place in the confined phase, including a preferential gauche conformation for EG in contrast to the characteristic trans conformation favored by longer PEO chains.

EXPERIMENTAL SECTION

Materials. *Synthesis of Graphite Oxide.* Graphite oxide was produced using natural graphite from Alfa Aesar (universal grade, 200-mesh, 99.9995% metal basis, reference number 40799). The starting graphite material was oxidized using a modified Brodie method.[4,26] Briefly, a reaction flask containing 200 mL of fuming nitric acid (Fluka) was cooled to 0 °C for 20 min using a cryostat bath, followed by the immersion of 10 g of graphite. Next, 80 g of potassium chlorate (Fluka) was slowly added over a period of 1 h in order to avoid sudden increases in temperature. The reaction mixture was stirred for 21 h at 0 °C. The mixture was then diluted in distilled water and filtered until the supernatant had a nitrate content below 1 mg/L (AQUANAL-plus nitrate (NO_3) 1−50 mg/L). The resulting GO slurry was dried at 80 °C for 24 h in a vacuum oven (P < 0.1 mbar) and stored in this oven at room temperature until further use. Elemental analysis of the so-obtained GO showed an atomic composition of stoichiometry $C_8H_{1.3}O_{2.6}$. Additional compositional information can be found in ref 4.

Preparation of Graphite−Oxide Intercalates. Triethylene glycol (3PEO) and pentaethylene glycol (5PEO) were purchased from Fluka, whereas EG and nPEO (with n = 13, 104, 795, and 2135) were supplied by Aldrich. nPEO/GO samples with $n \geq 13$ were prepared from aqueous solution by stirring a total of 0.5 g of PEO previously dissolved in 20 mL of water with 0.5 g of GO for 15 days. Any PEO excess was removed by filtration and thorough aqueous washings. The resulting PEO/GO specimen was then dried at 80 °C for 24 h in a vacuum oven (P < 0.1 mbar) connected to a dry scroll rotatory pump. PEO/GO, GO, and PEO were kept dry in the vacuum oven at room temperature prior to their physicochemical characterization. The intercalation of EG, 3PEO, and 5PEO (all of them are liquids at ambient temperature) was performed by direct mixing with GO in the absence of solvent. To remove any remaining liquid, the adduct was carefully rinsed with water and dried at 80 °C under vacuum. As precautionary measure, all samples were analyzed by TGA, DSC, and XRD to identify the presence of excess liquid. The drying procedure explained earlier was performed repeatedly to achieve the complete removal of the nonintercalated fraction. A final composition of ca. 22 ± 2 wt % EG(PEO) in the EG(PEO)/GO samples was ascertained by means of TGA and further corroborated by the INS measurements.

Characterization. *X-ray Diffraction.* XRD patterns were measured using both a Philips X'Pert Pro and a Bruker D8 Advance powder diffractometer. The first one is equipped with a secondary monochromator, Cu Kα radiation (λ = 1.54 Å) and a PIXcel solid-state detector. The second one is equipped with a Cu Kα radiation source (λ = 1.54 Å), a LynxEye detector and an Anton-Paar TTK450 temperature stage. The radiation source in both equipments was operated at a generator voltage of 40 kV and a current of 40 mA. XRD data were collected at 25 °C over the angular range 2θ = 5−60° with a stepsize of 0.026° in Bragg−Brentano parafocusing geometry.

Thermogravimetry. Thermogravimetry was carried out on a TA Instruments Q500 thermogravimetric analyzer. Samples were heated from room temperature to 600 at 1 °C/min under a constant N_2 flow of 60 mL/min. The amount of EG(PEO) in EG(PEO)/GO was calculated from sample-residue analysis at 450 °C, temperature at which the intercalated EG(PEO) undergoes decomposition (see the Supporting Information of ref 7). In this work, intercalated PEO in

dx.doi.org/10.1021/ma202655f | Macromolecules XXXX, XXX, XXX−XXX

GO was shown to decompose in two distinct stages at 214 and 295 °C by means of TGA/mass spectrometry. On the basis of this protocol, the amount of PEO in PEO/GO is given by $W_{PEO/GO} = f_{GO}W_{GO} + f_{PEO}W_{PEO}$, where $W_{PEO/GO}$, W_{GO}, and W_{PEO} are the weight percent of PEO/GO, GO, and PEO residues at 450 °C, respectively, and f_{GO} and f_{PEO} are the mass fractions of GO and PEO in PEO/GO, respectively. Since $f_{PEO} = 1 - f_{GO}$, we can write $f_{PEO} = (W_{GO} - W_{PEO/GO})/(W_{GO} - W_{PEO})$. The mass fraction of EG (f_{EG}) in EG/GO was calculated in a similar fashion via substitution of $W_{PEO/GO}(W_{PEO})$ by $W_{EG/GO}(W_{EG})$ in the last equation above.

Inelastic Neutron Scattering. INS data were collected on the TOSCA spectrometer[25] located at the ISIS Facility, Rutherford Appleton Laboratory, U.K. TOSCA is a so-called indirect geometry time-of-flight neutron spectrometer spanning an energy-transfer range up to 4000 cm^{-1} in neutron energy loss with a spectral resolution of ~1.5%. INS time-of-flight spectra were collected in both back- and forward-scattering geometries, and then added together to obtain hydrogen-projected VDOS's. Typical run times varied between 2 and 8 h depending on the hydrogen content of the sample. All samples were contained in flat aluminum cells of thickness 1−4 mm and cooled to temperatures below 30 K. On the basis of the thermal behavior of EG and *n*PEO observed by DSC, EG and *n*PEO with $n \geq 13$ cannot be obtained in an amorphous state, whereas the quenching of molten 3PEO and 5PEO in liquid nitrogen can prevent their crystallization. Thus, amorphous 3PEO and 5PEO were produced by direct immersion (quenching) in the TOSCA cryostat ($T < 30$ K). Crash cooling to cryogenic temperatures ($T < 100$ K) was optimized by placing the samples at the bottom of the cryostat and exposing them directly to a stream of liquid helium. To prepare a crystalline sample of 5PEO, the sample was first crystallized in a freezer at 240 K prior to its immersion in the low-temperature cryostat. INS data of GO, EG, and PEO were normalized to sample mass and those of EG(PEO)/GO were normalized to the amount of EG(PEO) content (about 22% of EG(PEO)/GO sample mass, as determined by TGA).

Differential Scanning Calorimetry. DSC measurements were carried out on ~12 mg specimens using a Q2000 TA Instruments in both standard and temperature-modulated (TM) modes. Standard DSC measurements were performed by placing the samples in sealed aluminum pans, holding the temperature for 10 min at 353 K, and cooling to 100 K at the highest attainable cooling rate. Bulk liquid samples at room temperature were quenched by immersing the sample in liquid nitrogen and then inserted into the DSC cell at 100 K. Bulk solid samples at room temperature were previously melted on a hot plate at 353 K before quenching. After the cooling run, all samples were heated back to 353 K in TM mode with a 0.48 K temperature amplitude, 60 s modulation period, and 3 K/min underlying heating rate. A helium flow rate of 25 mL/min was used all throughout.

Fourier Transform Infrared Spectroscopy. FTIR spectra were measured at room temperature over the range 700−4000 cm^{-1} with a JASCO 6500 spectrometer using an attenuated-total-reflectance (ATR) stage. Each spectrum was collected with a resolution of 4 cm^{-1} and an average of 200 repetitive scans. The spectra were neither baseline-corrected nor smoothed.

Raman Scattering. Unpolarised Raman scattering measurements were performed at room temperature in backscattering geometry over the energy-transfer range 100−3200 cm^{-1} (Stokes scattering). The Raman setup consisted of a bespoke Renishaw inVia Raman spectrometer equipped with a purpose-built fiber-coupled head to enable both offline as well as simultaneous neutron-Raman measurements. A 300 mW Toptica diode laser operating at a wavelength of 785 nm was used as excitation source. Raman spectra of EG, 3PEO, and 5PEO were recorded offline at room temperature. For more details of the experimental setup and measurement protocols, the reader is referred to ref 27.

RESULTS AND DISCUSSION

Effects of Molecular Size on Intercalate Structure. Owing to the hydrophilic character of the GO substrate, both EG and PEO intercalate into the GO galleries by diffusion either from aqueous solution or the bulk liquid. Moreover, *n*PEO chains with $n \geq 13$ were strongly retained by GO and further PEO recovery was not feasible by rinsing with water. A different behavior was observed for EG as well as the shorter 3PEO and 5PEO chains, which required careful control of sample-preparation conditions to avoid deintercalation. The amount of intercalated species ca. 22 ± 2 wt % was largely independent of molecular weight.

Graphite oxide is a paracrystalline material characterized by turbostratic layer stacking, i.e., irregular shifts and/or rotations of individual planes along the crystallographic *c*-axis. The layers are also irregular since the epoxide and hydroxyl groups and the remaining C=C double bonds are not distributed in a regular fashion within a given two-dimensional layer. As a result, the XRD data (see Figure 1a) typically display a prominent (001)

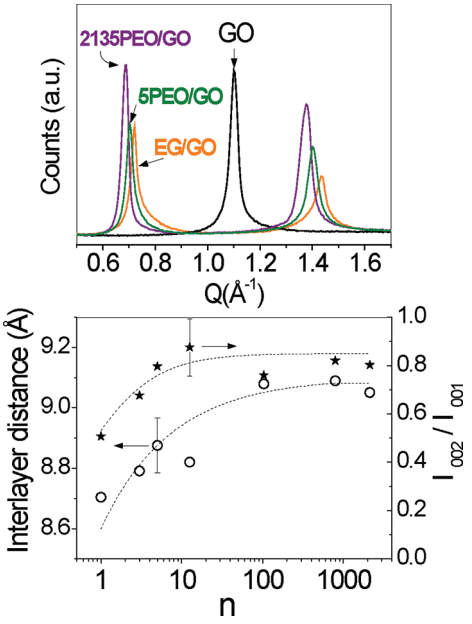

Figure 1. (a) XRD of GO as well as confined EG and *n*PEO with $n = 5$ and 2135 recorded on a Bruker D8 Advance powder diffractometer. (b) Left axis: Dependence of interlayer distance on the chain length of the intercalant (n). Right axis: 002 to 001 peak intensity ratio (I_{002}/I_{001}). The included error bars are a measure of the experimental uncertainties estimated from separate measurements by using different instruments and sample batches. Dashed lines are a guide to the eye.

reflection at 1.10 $Å^{-1}$ followed by a much weaker Bragg reflection (not shown) at 2.23 $Å^{-1}$ (002 line) indicative of in-plane ordering.[5] Representative XRD patterns of EG/GO, 5PEO/GO and 2135PEO/GO are also included in Figure 1a. The XRD patterns of EG/GO and *n*PEO/GO show two well-defined (001) and (002) reflections at 0.69−0.72 $Å^{-1}$ and 1.38−1.43 $Å^{-1}$, respectively, which account for the significant expansion of the GO interlayer along the crystallographic *c*-axis upon intercalation, from 5.7 Å to about 8.7−9.1 Å. After subtracting the 5.7 Å basal spacing of GO, the lattice expansion in (EG)PEO/GO corresponds to a space of approximately 3.0−3.4 Å, which suggests that both oligomers and long-chain polymers are arranged in a single molecular layer. For low-molecular-weight intercalants, the relative intensity of the 002 reflection was found to depend on chain length (see Figure 1b), as these species are more susceptible to adopt different spatial orientations within the GO interlayer. Thus, the observed increase in the intensity of the 002 relative to 001 peaks in

dx.doi.org/10.1021/ma202655f | *Macromolecules* XXXX, XXX, XXX−XXX

going from EG/GO to 13PEO/GO suggests a higher degree of order within the stacks[28] as a function of the molecular weight. This effect was not observed for chain lengths higher than n = 13.

Figure 1b also shows how the interlayer distance varies with chain length. As shown in the figure, the interlayer distance of the EG(PEO)/GO samples does not depend strongly on the chain length of the intercalate, further reinforcing the notion that the oligomer and polymer chains are forced to adopt a planar conformation in a monolayer arrangement, i.e., well-defined and extreme 2D confinement. The readily observable yet relatively small (~0.4 Å) variation in layer thickness from EG to the longest polymer with n = 2135 can be explained by the tendency of the smaller oligomers to adopt the same low-energy conformation as in the bulk, a condition that is harder to achieve for longer polymer chains. In this picture, the free-energy cost associated with achieving a perfectly (higher free-energy) planar conformation becomes significantly higher the longer the polymer chain, and, as result, the underlying GO substrate is forced to undergo a slight expansion.

Thermal Behavior. Figure 2 shows representative DSC profiles corresponding to EG, 3PEO, 5PEO, EG/GO, 3PEO/GO, and 5PEO/GO. Bulk 3PEO and 5PEO exhibit a step at 181 and 192 K, respectively, corresponding to the glass transition of the amorphous phases. Note that amorphous 3PEO and 5PEO can be readily obtained upon quenching, whereas EG crystallizes readily and its glass transition is hard to observe. These DSC thermograms also exhibit large exothermic and endothermic peaks at 224 (234) and 274 (262) K for 3PEO (5PEO), corresponding to the cold crystallization and further melting of crystalline domains in these oligomers. On the other hand, the DSC data for EG shows the presence of small and large endothermic peaks at 210 and 258 K, respectively, corresponding to the melting of two distinct crystalline phases in EG. However, EG/GO, 3PEO/GO, and 5PEO/GO do not show any signs of crystallization, melting, or glass transition. Instead, we only observe small deviations in heat flow compared to pristine GO, which arise from the contribution of the oligomeric species to the total heat flow. The absence of a distinct melting transition in these samples clearly indicates the impossibility of EG and PEO chains to crystallize when intercalated into GO, in agreement with previous studies on PEO intercalated in montmorillonite[24] and fluoromica-based clays.[9] No thermal events were detected for nPEO-mers with longer chain lengths (n = 13−2135), indicating that the organic phase is effectively accommodated in two dimensions irrespective of chain length.

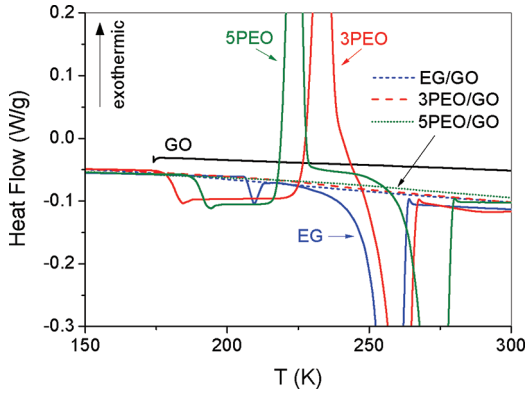

Figure 2. DSC profiles of GO, bulk EG, 3PEO, 5PEO as well as intercalated EG/GO, 3PEO/GO, and 5PEO/GO measured during heating at a rate of 3 K/min. Bulk materials were previously quenched by fast cooling to 100 K. For further details see the text.

Vibrational Spectroscopy. To investigate changes in molecular structure and macromolecular conformation upon confinement, INS measurements were performed on the TOSCA spectrometer on bulk EG(PEO) and EG(PEO)/GO at temperatures below 30 K. Since the most notable differences in the INS data were found for short-chain-length species, we will describe in detail the results for EG, 3PEO, and 5PEO. One of the primary advantages of INS spectroscopy is that there are no hard selection rules and mode intensities can be related to the underlying VDOS. Therefore, spectral assignments can be performed on the basis of our current knowledge and understanding of the vibrational spectrum of the bulk polymer obtained from optical spectroscopy[14,15,29] and computer simulation.[30] Another advantage of INS spectroscopy to characterize confined hydrogenous materials in GO stems from the strong neutron−proton incoherent cross section which dominates the INS response with minimal interference from the GO substrate. Last but not least, INS spectroscopy allows access to very low energy transfers below ~200 cm^{-1}, difficult to access with conventional infrared and Raman techniques.

Ethylene Glycol. INS spectra for GO, bulk EG, and EG/GO spanning the energy-transfer range 24−1600 cm^{-1} are shown in the lower panel of Figure 3. The GO spectrum exhibits a very weak and featureless INS response, which enables a clear identification of EG bands in the EG/GO sample. At higher energy transfers, the spectra only display a broad band associated with C−H stretching vibrations centered at 2935 cm^{-1} (see the Supporting Information). The integrated intensity of this high-energy feature corresponding to C−H stretch modes serves to validate the amount of EG in the sample (ca. 20 wt %), as detailed previously in ref 7 for the case of high-molecular-weight PEO/GO intercalates. Moreover, we find that this spectral feature does not suffer any changes in intensity or line shape upon confinement and can, therefore, be used as a reliable fingerprint of the total concentration of hydrogen in a given sample. On the basis of these observations,

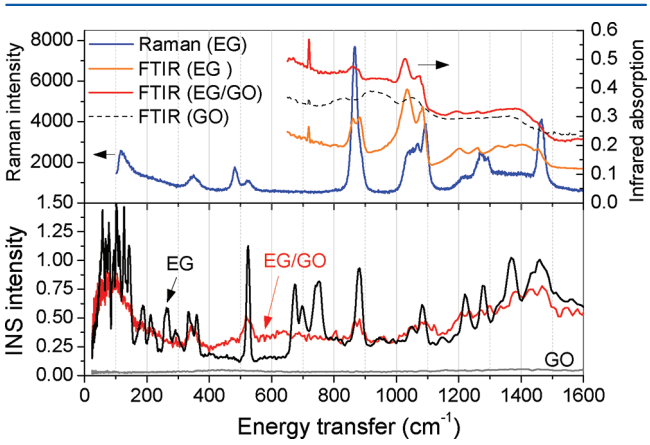

Figure 3. Top: Vibrational spectra of bulk EG, GO, and EG/GO obtained by FTIR spectroscopy and Raman scattering at room temperature. At this temperature, bulk EG is a liquid. Bottom: Mass-normalized INS spectra of GO, bulk crystalline EG, and confined EG/GO measured on the TOSCA spectrometer at 30 K.

dx.doi.org/10.1021/ma202655f | Macromolecules XXXX, XXX, XXX−XXX

intensity changes at lower energy transfers can then be linked to changes in the vibrational dynamics of the intercalate upon confinement.

The most significant differences between bulk and confined EG are observed at energy transfers below 1600 cm^{-1}. The INS data are characterized by the disappearance, shifting, and/or broadening of spectral bands in confined EG compared to the bulk. We can rationalize these results in terms of restricted EG motions within the 2D GO interlayer. Earlier spectroscopic studies have also examined the equilibrium between gauche and trans EG conformers in the bulk liquid and solid,[31,32] as well as confined in silica-glass pores of radii 3−7 nm.[33] These optical studies showed that the Raman bands at 522(480) cm^{-1} could be attributed to the gauche(trans) conformers (see also the Raman and FTIR spectra of liquid EG in the top panel of Figure 3). On the basis of the reported data, the band at 523 cm^{-1} in the INS spectrum of crystalline EG can be then attributed to the asymmetric CCO bending mode of the OCCO skeleton of the gauche conformer. Moreover, the absence of INS features centered around 482 cm^{-1} signals the absence of trans conformers in the crystalline state, in agreement with previous Raman studies on solid EG.[31] Therefore, the presence of a broad INS peak at 521 cm^{-1}, as well as the absence of a peak at 482 cm^{-1} for EG/GO suggests that EG is in a disordered gauche conformation in the confined state. This result is at odds with ref 33, where it was found that confinement of EG in silica-glass nanopores led to an increase of trans EG conformers. It is likely that the geometry as well as the chemical makeup of the silica pores play an important role in dictating the intramolecular structure of EG, as further corroborated in ref 33 after coating the silanol groups on the silica surface with hydrophobic molecules. In that case, the aforementioned changes in gauche−trans isomerism disappeared.

We also observe a decrease in INS peak intensities associated with CH_2 bends (1462 cm^{-1}), O−H in-plane bends (1430, 1369 cm^{-1}), CH_2 twisting modes coupled to wagging motions (1222, 1280 cm^{-1}), symmetric and antisymmetric CH_2−CH_2 rocking vibrations (1085 and 881 cm^{-1}, respectively), coupled vibrations of the C−C and C−O stretching modes (862 cm^{-1}, observed only in the FTIR spectrum), symmetric CCO bending modes (332, 360 cm^{-1}), as well as the absence of features associated with OH torsional modes and internal C−O rotations at 650−780 cm^{-1}.[31] These spectral changes qualitatively account for a strong reduction of EG vibrational motions upon confinement owing to an effective increase in proton effective mass and a concomitant redistribution of INS intensity away from the kinematic trajectories accessible on the TOSCA spectrometer. Such an overall decrease in proton mean-square displacements necessarily arises from a distinctly different local environment in the intercalated case and is amenable to further experimental verification as well as more detailed scrutiny as a function of temperature by quasielastic neutron scattering techniques. The broad INS signals below 300 cm^{-1} for confined EG also account for the suppression of complex collective modes, where the broad response below 160 cm^{-1} closely resembles the vibrational density of states of a disordered amorphous system. These results are also consistent with the DSC data reported in Figure 2, showing a clear suppression of crystalline phases upon confinement.

In the above context, the information offered by the FTIR data of confined EG (top panel in Figure 3) is rather limited due to the extensive overlap of EG and GO contributions in the composite system. Nonetheless, a comparison of the FTIR spectrum of EG/GO with that of liquid EG indicates a red shift of symmetric CH_2−CH_2 rocking vibrations (1085 cm^{-1}) and C−C stretch modes (1034 cm^{-1}), which can be related to conformational changes in the confined EG phase. Figure 4 highlights the spectral region of the FTIR data where the most significant changes occur. These correspond to the OH-stretch region at ca. 3000−3650 cm^{-1}, associated with the presence of OH groups in both EG and GO substrate. The red shift observed in going from pristine GO to EG/GO indicates the formation of intermolecular hydrogen-bonds between OH groups in GO and EG, and are associated with an overall weakening of GO O−H bonds. A similar behavior is found in the 3PEO/GO and 5PEO/GO samples, indicating that 3PEO and 5PEO are also able to form hydrogen bonds with the substrate. Moreover, the presence of a shoulder at 3540 cm^{-1} in EG/GO hints at the rupture of intermolecular hydrogen bonds in EG and the formation of new intramolecular hydrogen bonds or free OH groups in the composite material. This spectral assignment is based on a previous study of OH stretch vibrations for EG in CCl_4 solutions.[31] It is noteworthy that the shoulder at 3540 cm^{-1} disappears as the chain length increases to 3PEO and 5PEO. This result indicates that accessibility to the oxygen-containing functional groups in GO, capable of forming hydrogen bonds with the intercalant (e.g., OH, epoxy, carbonyl, carboxyl, etc.), is favored for longer molecular chains than for a small molecule. As a result, some terminal OH groups in EG cannot bind to the GO substrate and appear as free or as intramolecular OH bonds. On the basis of our spectroscopic observations, Figure 5 depicts several hydrogen-bonding scenarios applicable to EG/GO, including the possibility of free OH groups in intercalated EG. The

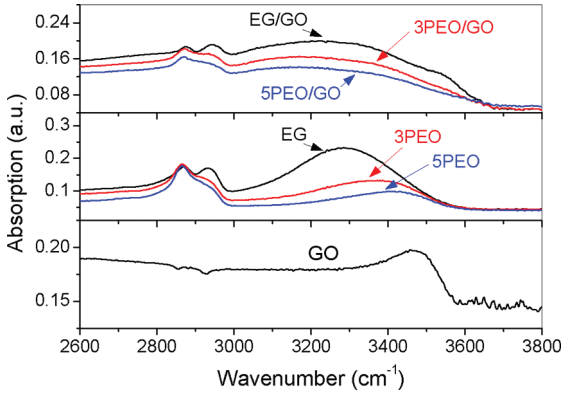

Figure 4. ATR-FTIR spectra of GO as well as of bulk and intercalated EG, 3PEO, and 5PEO at 298 K.

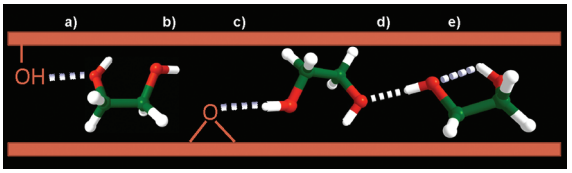

Figure 5. Schematic diagram of hydrogen-bond interactions in EG/GO inferred from the spectroscopic data: (a, c) intermolecular bonds between EG and GO; (d) intermolecular bonds between two EG molecules; and (e) intramolecular EG bonds. Part b signifies the presence of dangling OH groups.

dx.doi.org/10.1021/ma202655f | Macromolecules XXXX, XXX, XXX−XXX

concentration of these dangling OH groups must in turn be related to the degree of oxidation and chemical topology of the underlying GO substrate. This observation alone suggests yet another relatively unexplored means of controlling intra- and intermolecular intercalant geometry in this family of composite materials.

Poly(ethylene oxide). The vibrational spectra for 3PEO, 5PEO, and their confined counterparts are shown in Figure 6

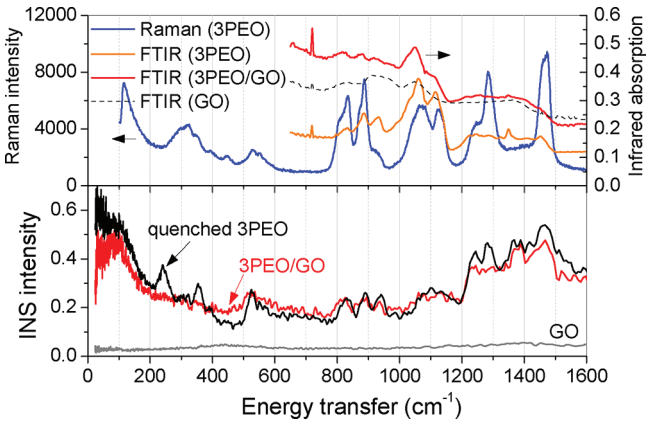

Figure 6. Top: Vibrational spectra of bulk 3PEO, GO, and 3PEO/GO obtained by FTIR spectroscopy and Raman scattering at room temperature. At this temperature, 3PEO is a liquid. Bottom: Mass-normalized INS spectra of GO, crystalline 3PEO, and 3PEO/GO measured on the TOSCA spectrometer at 30 K.

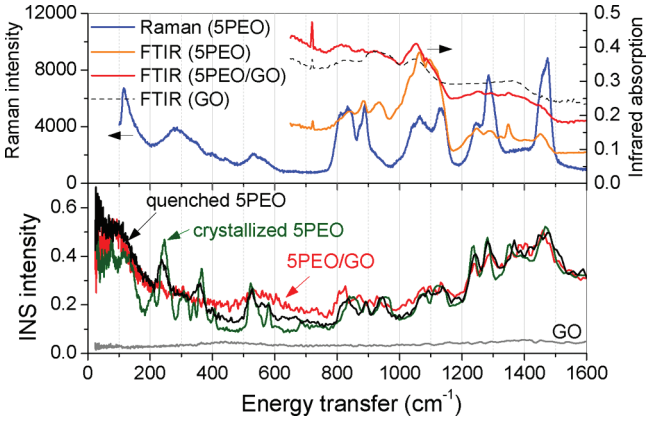

Figure 7. Top: Vibrational spectra of bulk 5PEO, GO, and 5PEO/GO obtained by FTIR spectroscopy and Raman scattering at room temperature. At this temperature, 5PEO is a liquid. Bottom: Mass-normalized INS spectra of GO, quenched 5PEO, crystalline 5PEO, and 5PEO/GO measured on the TOSCA spectrometer at 30 K.

and Figure 7. Similarly to EG/GO, not much information about the structure of 3PEO(5PEO) can be extracted from the FTIR data of 3PEO/GO(5PEO/GO) due to the strong infrared absorption of GO and the limited energy range of our FTIR equipment. The most significant feature in the FTIR spectra is the red shift of C−O−C stretching vibrations from ∼1061 cm^{-1}[29] (bulk 3PEO and 5PEO) to ∼1050 cm^{-1} (3PEO/GO and 5PEO/GO), associated with the formation of hydrogen bonds between PEO chains and the substrate.

The INS spectra of Figure 6 show striking similarities in terms of relative intensities in quenched bulk 3PEO and 3PEO/GO, although some peaks in 3PEO/GO are shifted, absent, or broadened. All of these findings suggest an amorphous-like confined phase for 3PEO as well. In contrast to the sharp peaks observed in the INS spectrum of EG (cf. Figure 3), the vibrational bands of bulk 3PEO are clearly broader and of lower intensity owing to the fact that 3PEO was effectively quenched during the insertion of the liquid sample into the TOSCA cryostat. As mentioned earlier, the strong tendency of EG to crystallize, even upon quenching, did not allow a measurement of amorphous EG using the experimental protocol described in previous sections. Instead, Figure 7 shows the results of a further INS experiment to explore differences in vibrational spectra between the amorphous and crystalline states of 5PEO. The most noticeable changes when comparing the bulk and confined PEO samples, or the amorphous and crystalline 5PEO bulk, lie in the region below 1000 cm^{-1}. The intensity and peak position of the bands observed in this region are particularly sensitive to chain conformation (i.e., trans and gauche conformers) which, in turn, are also affected by temperature, dilution, metal coordination, and geometrical constraints.[7,13−16,29]

At lower energy transfers, the region around 780−970 cm^{-1} is dominated by the presence of CH_2 rocking modes. Amorphous 3PEO and 5PEO show three bands at 831, 890, and 943 cm^{-1} in the INS spectra at nearly the same energies as in the FTIR and Raman spectra of liquid 3PEO and 5PEO, a result that is consistent with the liquid (amorphous) bulk-like behavior of quenched 3PEO and 5PEO. The bands at 831 cm^{-1} show a characteristic blue/red shift for the crystalline/confined 5PEO sample (cf. Figure 7). These spectral shifts are directly related to the appearance of new conformational structures in the different phases. In crystalline PEO, the band at 846 cm^{-1} has been assigned to trans−gauche−trans (*tgt*) conformations of CCOC, OCCO, and COCC groups.[14] For the amorphous phase, there appears to be a sensible increase in the population of trans conformers, reaching a maximum in the confined PEO phase. The band at 816 cm^{-1} appearing in 3PEO/GO and 5PEO/GO has been assigned to CH_2 rocking modes associated with trans−trans−trans (*ttt*) geometries.[14] This assignment is further corroborated by the red shift and intensity suppression of the peak at 953 cm^{-1} in crystalline 5PEO, corresponding to trans−gauche−trans (*tgt*) conformations in the crystal. These results are firm evidence that confined 5PEO is in a different arrangement than that found in the liquid or crystalline bulk phases.

In addition to the above, the INS and Raman band at 890 cm^{-1} decreases in intensity with increasing chain length from n = 3−5 (see Figure 6 and Figure 7) and disappears for $n \geq 13$ (Figure 8). Moreover, the INS band intensity at 890 cm^{-1} does not change in going from the amorphous to the crystalline state in bulk 5PEO. This band has been assigned to CH_2 rocking modes of *tgg* and *ggg* conformations.[14] However, on the basis of the present results, this band could also be associated with the chain end groups. Previous studies have assigned the chain end groups to be a peak at either 811[16] or 830 cm^{-1},[14,30] both of them being very sensitive to the crystalline or amorphous state of the polymer.

The changes in the longitudinal-acoustic-mode (LAM) region (200−400 cm^{-1})[30] reported in Figure 7 provide more evident signatures of changes in macromolecular conformation. These bands correspond to complex modes associated with collective vibrations along the polymer chain. Crystalline 5PEO shows several well-defined spectral features in this region

dx.doi.org/10.1021/ma202655f | *Macromolecules* XXXX, XXX, XXX−XXX

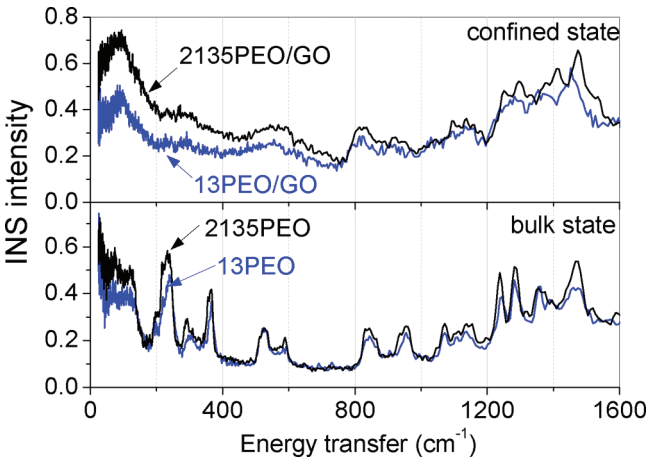

Figure 8. Comparison of mass-normalized INS spectra for bulk and confined *n*PEO with n = 13 and 2135, measured on the TOSCA spectrometer at 30 K.

centered at 210, 246, 308, 340, 364, and 405 cm^{-1}, whereas in the amorphous bulk material only the peaks at 240 and 358 cm^{-1} can be discerned. Earlier experimental and theoretical Raman studies have explained these changes as a result of distinct conformational distributions of the PEO chain.[30] These authors obtained simulated Raman spectra for different combination sequences involving nine rotameric states (i.e., *tgt*−*tgg*−*ttt*, *ttt*−*ttt*−*ttt*, etc.) and observed distinct patterns for each configuration, which were strongly dependent on the exact sequence of rotameric states rather than on the fractional content of *t*, *g*, and *g*′ states. They also determined that the *tgg*′ conformer was favored in molten PEO and that it displayed characteristic bands at 350 and 830 cm^{-1}. Indeed, our INS spectrum of amorphous 5PEO shows the presence of these two bands, the first barely discernible in the Raman data of liquid 5PEO in Figure 7. It is noteworthy that most of the experimental and theoretical studies of the vibrational density of states of PEO are related to *n*PEO with $n \geq 13$, with the notable exception of EG which has been the subject of numerous studies as well. For shorter chain lengths, it is rather difficult to assign the peaks observed in the LAM region without detailed theoretical models. For instance, by comparing the INS spectra of crystalline 5PEO in Figure 7 to those corresponding to *n*PEO with n = 13 and 2135 in Figure 8, it becomes apparent that vibrational modes in the LAM region depend quite sensitively on chain length. The first one shows 6 LAM bands whereas the latter two show only 4. Moreover, the LAM-mode region as well as the entire spectrum for *n*PEO with n = 13 and 2135 are identical except for overall intensity changes arising from differences in hydrogen content for each sample. These results account for the relative importance of the chain ends to the overall configurational structure of the PEO chains, which become less relevant for chain lengths larger than $n \geq 13$.

In the confined state, the absence of peaks in the LAM region for all PEO chains as compared to their bulk counterparts is quite apparent (cf. Figures 6−8). Such a result is largely insensitive to molecular size and suggests the emergence of a new set of chain length scales primarily dictated by the presence of anchoring points on the GO substrate upon intercalation. In the case of confined EG, the persistence of the band at 344 cm^{-1}, which has been found to be independent(dependent) of temperature in the confined (bulk) phase,[34] could be associated with end-group vibrations. These results are a firm indication of a local reduction of vibrational motions of PEO chains within the GO interlayer. A detailed theoretical model taking proper account of the presence of an essentially disordered array of intercalant-substrate hydrogen bonds is, however, required to further quantify the observed and rather stark changes to polymer properties, including a conspicuous absence of LAM-like features in the INS data as well as a sensible reduction in vibrational motion upon intercalation.

CONCLUSIONS

The present work has shown that confinement of EG and *n*PEO (n = 3, 5, 13, 104, 795, and 2135) in GO interlayers induces profound changes to the dynamics and structure of the confined organic phase. Both crystallization and calorimetric glass transition in EG and PEO are inhibited as a result of strong geometric restrictions. Likewise, the INS data unequivocally show that chain conformations are distinctly different from those characteristic of their crystalline and amorphous bulk counterparts. These findings can be related to the extreme 2D confinement (3−3.4 Å), as well as to the role of hydrogen-bonding interactions between intercalant and GO substrate. INS spectroscopy has provided unique insights into the vibrational and conformational properties of the confined phase, and served to confirm the presence of ca. 22 ± 2 wt % intercalant in these composite materials. The disappearance of LAM-like modes in all confined PEO chains and the persistence of a well-defined band at 340 cm^{-1} for confined EG suggest that further control of polymer properties may be achieved via a judicious tuning of the chemical composition and topology of the underlying GO substrate.

ASSOCIATED CONTENT

Supporting Information

Inelastic neutron scattering results at high energy transfer and resume of the INS bands for bulk and confined EG and *n*PEO materials. This material is available free of charge via the Internet at http://pubs.acs.org/

AUTHOR INFORMATION

Corresponding Author

*E-mail: fbarroso@ehu.es. Telephone: +34 94301 8803. Fax: +34 94301 5800.

Notes

The authors declare no competing financial interest.

ACKNOWLEDGMENTS

The authors gratefully acknowledge the support of the Spanish Ministry of Education (MAT2007-63681), the Basque Government (IT-436-07), and the U.K. Science and Technology Facilities Council for beamtime on the TOSCA spectrometer and access to the Raman spectrometer in the ISIS Sample Characterisation Laboratory. F.B.-B. acknowledges a JAE-Doc contract from CSIC. F.F.-A. acknowledges financial support from the U.K. Science and Technology Facilities Council. We thank Dr. A. Larrañaga from SGIker UPV/EHU for the XRD measurements on the Philips X'Pert Pro powder diffractometer.

REFERENCES

(1) Jackson, C. L.; McKenna, G. B. *J. Chem. Phys.* **1990**, *93*, 9002−9011.

(2) Jackson, C. L.; McKenna, G. B. *J. Non-Cryst. Solids* **1991**, *131*−*133*, 221−224.
(3) Alcoutlabi, M.; McKenna, G. B. *J. Phys.-Condes. Matter* **2005**, *17*, R461−R524.
(4) Cerveny, S.; Barroso-Bujans, F.; Alegría, A.; Colmenero, J. *J. Phys. Chem. C* **2010**, *114*, 2604−2612.
(5) Barroso-Bujans, F.; Cerveny, S.; Alegría, A.; Colmenero, J. *Carbon* **2010**, *48*, 3277.
(6) Barroso-Bujans, F.; Cerveny, S.; Verdejo, R.; del Val, J.; Alberdi, J.; Alegría, A.; Colmenero, J. *Carbon* **2010**, *48*, 1079−1087.
(7) Barroso-Bujans, F.; Fernandez-Alonso, F.; Cerveny, S.; Parker, S. F.; Alegría, A.; Colmenero, J. *Soft Matter* **2011**, *7*, 7173−7176.
(8) Harris, D. J.; Bonagamba, T. J.; Schmidt-Rohr, K. *Macromolecules* **1999**, *32*, 6718.
(9) Miwa, Y.; Drews, A. R.; Schlick, S. *Macromolecules* **2008**, *41*, 4701−4708.
(10) Jeevanandam, P.; Vasudevan, S. *Chem. Mater.* **1998**, *10*, 1276−1285.
(11) Tunney, J. J.; Detellier, C. *Chem. Mater.* **1996**, *8*, 927−935.
(12) Aranda, P.; Ruiz-Hitzky, E. *Chem. Mater.* **1992**, *4*, 1395−1403.
(13) Papke, B. L.; Ratner, M. A.; Shriver, D. F. *J. Phys. Chem. Solids* **1981**, *42*, 493−500.
(14) Maxfield, J.; Shepherd, I. W. *Polymer* **1975**, *16*, 505−509.
(15) Matsuura, H.; Miyazawa, T. *J. Polym. Sci., Part A2: Polym. Phys.* **1969**, *7*, 1735−1744.
(16) Koenig, J. L.; Angood, A. C. *J. Polym. Sci., Part A2: Polym. Phys.* **1970**, *8*, 1787−1796.
(17) Wong, S.; Zax, D. B. *Electrochim. Acta* **1997**, *42*, 3513−3518.
(18) Mitchell, P. C. H.; Parker, S. F.; Ramirez-Cuesta, A. J.; Tomkinson, J. *Series on Neutron Techniques and Applications. Vibrational Spectroscopy with Neutrons: with Applications in Chemistry, Biology, Materials Science and Catalysis*; World Scientific: London, 2005.
(19) Hackett, E.; Manias, E.; Giannelis, E. P. *Chem. Mater.* **2000**, *12*, 2161−2167.
(20) Yang, G.; Hou, W.; Sun, Z.; Yan, Q. *J. Mater. Chem.* **2005**, *15*, 1369−1374.
(21) Liu, Y. J.; DeGroot, D. C.; Schindler, J. L.; Kannewurf, C. R.; Kanatzidis, M. G. *Chem. Mater.* **1991**, *3*, 992−994.
(22) Lemmon, J. P.; Lerner, M. M. *Chem. Mater.* **1994**, *6*, 207−210.
(23) Elmahdy, M. M.; Chrissopoulou, K.; Afratis, A.; Floudas, G.; Anastasiadis, S. H. *Macromolecules* **2006**, *39*, 5170.
(24) Vaia, R. A.; Sauer, B. B.; Tse, O. K.; Giannelis, E. P. *J. Polym. Sci., Part B: Polym. Phys.* **1997**, *35*, 59−67.
(25) Colognesi, D.; Celli, M.; Cilloco, F.; Newport, R. J.; Parker, S. F.; Rossi-Albertini, V.; Sacchetti, F.; Tomkinson, J.; Zoppi, M. *Appl. Phys. A—Mater. Sci. Process* **2002**, *74*, s64.
(26) Barroso-Bujans, F.; Alegría, A.; Colmenero, J. *J. Phys. Chem. C* **2010**, *114*, 21645−21651.
(27) Adams, M. A.; Parker, S. F.; Fernandez-Alonso, F.; Cutler, D. J.; Hodges, C.; King, A. *Appl. Spectrosc.* **2009**, *63*, 727−732.
(28) Vaia, R. A.; Liu, W. *J. Polym. Sci., Part B: Polym. Phys.* **2002**, *40*, 1590−1600.
(29) Yoshihara, T.; Tadokoro, H.; Murahashi, S. *J. Chem. Phys.* **1964**, *41*, 2902−2911.
(30) Yang, X.; Su, Z.; Wu, D.; Hsu, S. L.; Stidham, H. D. *Macromolecules* **1997**, *30*, 3796−3802.
(31) Matsuura, H.; Miyazawa, T. *Bull. Chem. Soc. Jpn.* **1967**, *40*, 85−94.
(32) Matsuura, H.; Hiraishi, M.; Miyazawa, T. *Spectrochim. Acta, Part A* **1972**, *28*, 2299−2304.
(33) Luo, R.; Jonas, J. *J. Raman Spectrosc.* **2001**, *32*, 975−978.
(34) Crupi, V.; Majolino, D.; Migliardo, P.; Venuti, V. *J. Chem. Phys.* **2003**, *118*, 5971−5978.